Article

Setting up In$_2$O$_3$-ZrO$_2$/SAPO-34 Catalyst for Improving Olefin Production via Hydrogenation of CO$_2$/CO Mixtures

Ander Portillo *, Onintze Parra, Andrés T. Aguayo, Javier Ereña, Javier Bilbao and Ainara Ateka *

Department of Chemical Engineering, University of the Basque Country UPV/EHU, P.O. Box 644, 48080 Bilbao, Spain
* Correspondence: ander.portillo@ehu.eus (A.P.); ainara.ateka@ehu.eus (A.A.); Tel.: +34-94-6015341 (A.A.)

Abstract: The adequate configuration and the effect of the reduction was studied for the In$_2$O$_3$-ZrO$_2$/SAPO-34 catalyst with the aim of improving its performance (activity and selectivity in the pseudo-steady state) for the hydrogenation of CO, CO$_2$ and CO$_2$/CO (CO$_x$) mixtures into olefins. The experiments were carried out in a packed bed reactor at 400 °C; 30 bar; a H$_2$/CO$_x$ ratio of 3; CO$_2$/CO$_x$ ratios of 0, 0.5 and 1; a space time (referred to as In$_2$O$_3$-ZrO$_2$ catalyst mass) of 3.35 g$_{InZr}$ h mol$_C{}^{-1}$; and a time on stream up to 24 h. The mixture of individual catalyst particles, with an SAPO-34 to In$_2$O$_3$-ZrO$_2$ mass ratio of 1/2, led to a better performance than hybrid catalysts prepared via pelletizing and better than the arrangement of individual catalysts in a dual bed. The deactivation of the catalyst using coke deposition and the remnant activity in the pseudo-steady state of the catalyst were dependent on the CO$_2$ content in the feed since the synergy of the capabilities of the SAPO-34 catalyst to form coke and of the In$_2$O$_3$-ZrO$_2$ catalyst to hydrogenate its precursors were affected. The partial reduction of the In$_2$O$_3$-ZrO$_2$/SAPO-34 catalyst (corresponding to a superficial In^0/In$_2$O$_3$ ratio of 0.04) improved its performance over the untreated and fully reduced catalyst in the hydrogenation of CO to olefins, but barely affected CO$_2$/CO mixtures' hydrogenation.

Keywords: CO$_2$; In$_2$O$_3$ catalyst; SAPO-34 catalyst; methanol synthesis; olefin synthesis; coke deactivation

1. Introduction

The production of light olefins from biomass gasification-derived syngas and CO$_2$ receives great attention to achieve the objective of net-zero carbon emissions by 2050 [1], and their industrial implementation is conditioned to the availability of green H$_2$ obtained from renewable energy [2]. The increasing demand of light olefins due to their use as key building blocks in the chemical industry justifies this initiative [3], replacing the technologies of the steam cracking of oil fractions [4], fluidized catalytic cracking (FCC) [5] and the conversion of methanol (MTO process) [6], which lead to large CO$_2$ emissions.

The direct conversion of CO, CO$_2$ and CO$_2$/CO mixtures into olefins can proceed via two different routes with tandem catalysts. In the modified Fischer–Tropsch (MFT) route, an acid zeolite is added to the FT catalyst (based on Fe or Co) for the selective conversion into olefins of the higher-hydrocarbon product of the FT synthesis (with characteristic Anderson–Schulz–Flory (ASF) distribution) [7,8]. The route with oxygenates (methanol/DME) as intermediates proceeds over oxide/zeotype (OX/ZEO) tandem catalysts, composed of a metallic oxide for the synthesis of oxygenates and a zeotype for their conversion into olefins. The attractiveness of these direct olefin synthesis routes lies in the lower infrastructure requirement compared with the two-stage processes and in the reduction of the thermodynamic limitations of the intermediates' (methanol/DME) formation. This advantage is a consequence of the shift in the equilibrium of their formation (Equations (1)–(3)) due to their in situ conversion, mainly into olefins (Equation (4)).

$$CO + 2\,H_2 \rightleftharpoons CH_3OH \tag{1}$$

$$CO_2 + 3\,H_2 \rightleftharpoons CH_3OH + H_2O \tag{2}$$

$$2\,CH_3OH \rightleftharpoons CH_3OCH_3 + H_2O \tag{3}$$

$$CH_3OH/CH_3OCH_3 \rightarrow \text{light olefins} \rightarrow \text{light paraffins + higher hydrocarbons + coke} \tag{4}$$
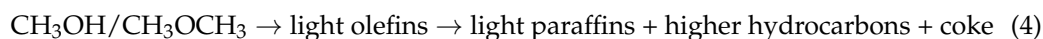
Moreover, the thermodynamics of the direct olefin formation also depend on the composition of the feed, being favored by co-feeding CO with CO_2 [9]. The concentration of both components is related by the extent of the water–gas shift (WGS) reaction (Equation (5)).

$$CO + H_2O \rightleftharpoons CO_2 + H_2 \tag{5}$$

The design of new tandem catalysts that are active, selective and stable under these conditions is of priority interest [10,11]. The suitable performance of the In_2O_3-ZrO_2/SAPO-34 catalyst is a consequence of the performance of each of the individual catalysts in the reaction stages. The significant activity of In_2O_3 for the step of methanol synthesis (Equations (1)–(2)) is related to the capacity of their surface oxygen vacancies for CO and CO_2 adsorption and H_2 dissociation [12,13]. The cyclic generation and annihilation of oxygen vacancies and their role in the methanol formation mechanism were investigated through density functional theory (DFT) studies on the hydrogenation of CO_2 over both non-defective [14] and defective [15] In_2O_3 (110) surfaces. These studies emphasized the ability of the In_2O_3 catalyst to suppress the reverse water–gas shift (rWGS) reaction. Experimental results presented by Sun et al. [16] using a commercial In_2O_3 catalyst demonstrated its activity in methanol synthesis, albeit with moderate yields. Martin et al. [17] showed that the activity of the catalyst could be significantly enhanced by selecting optimal reaction conditions, co-feeding CO and incorporating ZrO_2, as later confirmed by [18–21]. According to these authors, the adsorbed CO and CO_2 interact with active H* species, leading to the formation of formate (HCOO*) and methoxy (H_3CO*) intermediates, which ultimately undergo hydrogenation steps to produce methanol [22]. Recently, an extensive review on In_2O_3-based catalysts for the hydrogenation of CO_2 to methanol was conducted by Cai et al. [23].

SAPO-34 silicoaluminophosphate has been ascertained as the appropriate acid catalyst for the in situ selective conversion of methanol into DME (Equation (3)) and of methanol/DME into olefins (Equation (4)) [24–26]. The dual cycle mechanism, with polymethyl benzenes and olefins as intermediates, is well-established [27]. The high light-olefin selectivity obtained with this catalyst is based on its porous structure (CHA morphology, with eight-membered ring pore openings of 0.38×0.38 nm and cavities of 0.67×0.94 nm) and the high density of its acid sites of moderate strength [28], limiting the conversion of light olefins to other hydrocarbons. The synergy in the In_2O_3-ZrO_2/SAPO-34 tandem catalyst shows promising results, attaining a CO_2 conversion of almost 5-fold that with the In_2O_3-ZrO_2 catalyst [19].

Gao et al. [29] studied the effect of the SAPO-34 to In_2O_3 mass ratio on the selectivity of light olefins with hybrid catalysts (prepared via the joint pelletizing of In_2O_3 and SAPO-34 catalysts) and obtained different results for the hydrogenation of CO and CO_2. These authors also assessed the effect of the tandem catalyst's preparation (physical mixture or pelletizing of the individual catalysts) on olefin selectivity for CO_2/H_2 feeds [30].

An important challenge for the In_2O_3-ZrO_2/SAPO-34 tandem catalyst is controlling its deactivation, which has received minor attention in the literature. The fast coke deposition on SAPO-34 has been ascertained to be the cause for deactivation. After this, the catalyst acquires a pseudo-steady state of remarkable remnant activity for olefin formation [26,31]. This pseudo-steady state is interesting for the use of the catalyst at a greater scale and is related to the activity of In_2O_3-ZrO_2 for the hydrogenation of coke precursors.

Another challenge for the use of In_2O_3-ZrO_2/SAPO-34 tandem catalysts relies on determining whether a total or partial reduction of the catalyst is adequate for its optimal performance. The reported results reveal notable discrepancies in the interest in the reduction for different authors. It improves the performance under certain reaction conditions, either because the formation of In-H hydride is favored, which is an intermediate for methanol formation [20], or because In_2O_{3-x} corresponds to the most catalytically active state [12]. However, no improvement is observed under other conditions [32,33]. Indeed, the undesired over-reduction of In, easing its sintering and causing the consequent irreversible deactivation of the catalyst, has also been established [12,21]. These discrepancies in the effect of catalyst reduction can be attributed to the differences in the preparation and composition of the tandem catalysts, but also to differences in the feed composition and reaction conditions. Moreover, not considering catalyst deactivation may hamper the understanding and leads to obtaining different results.

Attending to the effect of the tandem catalyst configuration [30] and its arrangement in the reactor [34] in the synthesis of olefins from CO_2/CO, in this work, different original features regarding the In_2O_3-ZrO_2/SAPO-34 tandem catalyst were studied, which are important to fill a notable knowledge gap for the hydrogenation of CO_2/CO into olefins. Taking into account the rapid deactivation of the catalyst, attention has been focused on optimizing the results in the pseudo-steady state due to its interest on a larger scale. In different sections, the following were studied: (i) the SAPO-34 to In_2O_3-ZrO_2 mass ratio; (ii) the adequate configuration for the tandem catalyst; and (iii) the adequacy of the oxidation–reduction state of the In_2O_3-ZrO_2 catalyst. Thus, the topics studied seek to improve the synergy of the reaction steps of methanol/DME synthesis and their conversion into olefins.

2. Results and Discussion

The mass ratio between SAPO-34 and In_2O_3-ZrO_2 in the tandem catalysts, the configuration of the catalyst (mixed or hybrid) and of the catalytic bed (single or dual) and the effect of the catalysts' reduction treatment (partial or complete) were studied successively.

2.1. Optimal SAPO-34 to In_2O_3-ZrO_2 Ratio

The effect of the SAPO-34 to In_2O_3-ZrO_2 mass ratio in the catalyst was studied for the three representative mixtures in the feed: H_2/CO (CO_2/CO_x of 0), H_2/CO_2/CO (CO_2/CO_x of 0.5) and H_2/CO_2 (CO_2/CO_x of 1). In order to facilitate the comparison, the same In_2O_3-ZrO_2 catalyst amount in all experiments (corresponding to a space time of 3.35 g_{InZr} h mol_C^{-1}) was used. The space time is defined as the ratio between the catalyst mass and the CO_2/CO molar flow rate in the feed. Thus, the ratio between 1.22×10^{-1} g of the In_2O_3-ZrO_2 catalyst and 3.68×10^{-2} mol of CO_2/CO h^{-1} was used. In Figure 1, the effect of the SAPO-34 to In_2O_3-ZrO_2 ratio over the products' yield is presented for the H_2/CO feed. The results correspond to 16 h on stream (that is, in the pseudo-steady state, as shown later in the results regarding deactivation). As observed, the olefin yield boosted and surpassed 3% for an SAPO-34 to In_2O_3-ZrO_2 ratio of 0.5 and showed a plateau for higher SAPO-34 contents. However, an undesired increase in paraffin yield was also observed. This result is attributable to the conversion of olefins through hydrogen transfer reactions activated by the acid sites of SAPO-34 [35]. Consequently, the olefin yield achieved with a SAPO-34 to In_2O_3-ZrO_2 ratio of 0.5 and a selectivity of ~60% was not improved, further increasing the amount of SAPO-34. Similar trends of product-yield evolution with this SAPO-34 to In_2O_3-ZrO_2 ratio were observed for ternary (H_2/CO/CO_2) feeds and H_2/CO_2 feeds (Figures S1a and S1b in the Supplementary Materials, respectively). Consequently, the SAPO-34 to In_2O_3-ZrO_2 ratio of 0.5 is suitable to obtain an adequate combination of activity, selectivity and stability of the catalyst, as a consequence of the synergy in the extent of the stages of methanol synthesis and its conversion into olefins, and of the control of the coke deposition on SAPO-34.
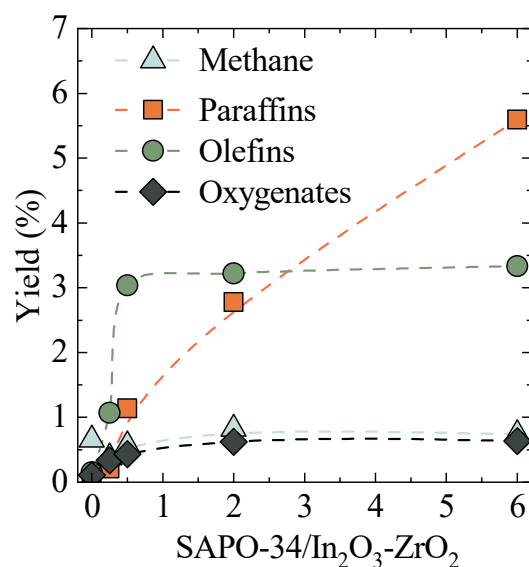
Figure 1. Effect of SAPO-34 to In_2O_3-ZrO_2 mass ratio in the tandem catalyst on product yields. Reaction conditions: feed, H_2/CO; 400 °C; 30 bar; H_2/CO_x, 3; CO_2/CO_x, 0; time on stream, 16 h; space time, 3.35 g_{InZr} h mol_C^{-1}.

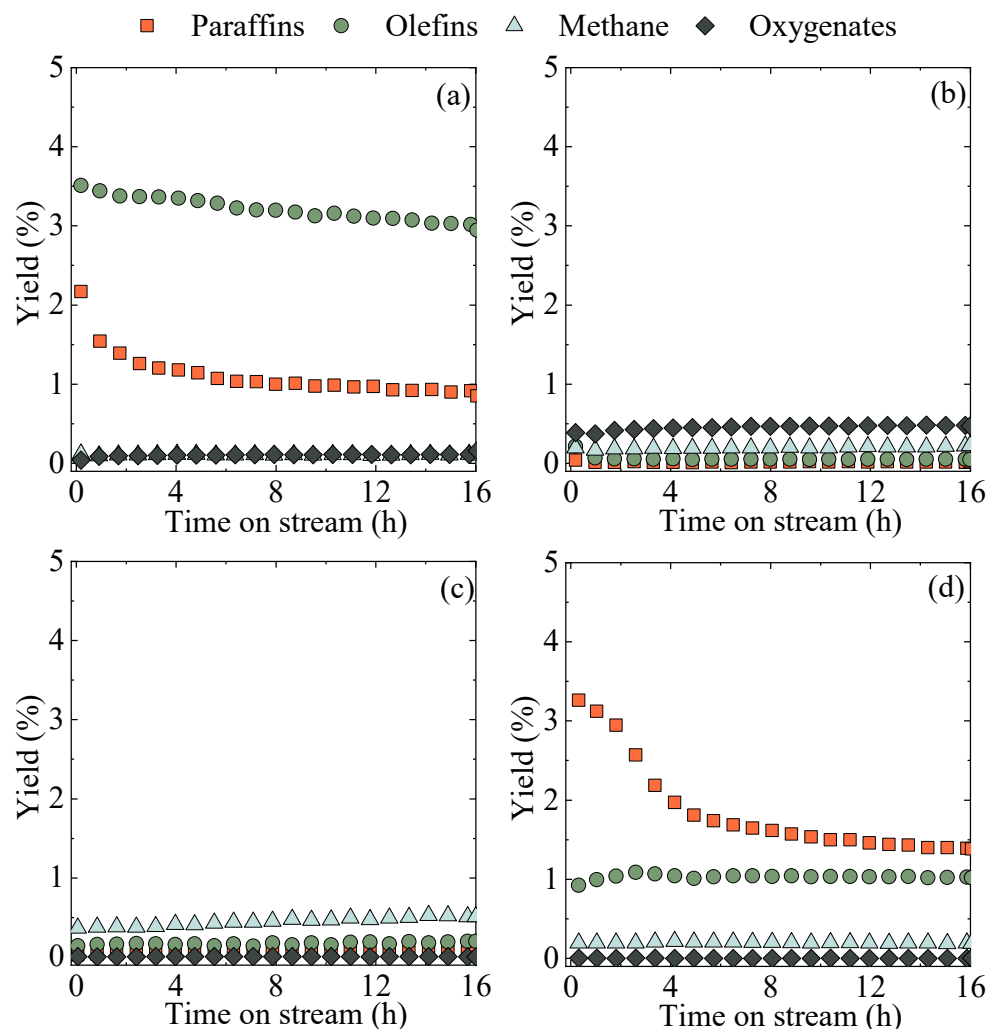## 2.2. Configuration of the Catalyst and Catalytic Bed

The catalyst composition selected in the previous section (SAPO-34 to In_2O_3-ZrO_2 ratio of 0.5) was tested for different configurations (described in Figure 2): (a) a packed bed with a physical mixture of In_2O_3-ZrO_2 and SAPO-34 particles (as described in Section 3.1); (b) a packed bed with an In_2O_3-ZrO_2/SAPO-34 hybrid catalyst prepared via the mortar mixing of both catalysts and the subsequent pelletizing of the mixture (Section 3.1); (c) a dual packed-bed configuration, placing first an In_2O_3-ZrO_2 bed and, subsequently, an SAPO-34 bed; and (d) a dual packed bed, the first with a tandem catalyst with configuration (a) and, subsequently, an additional bed with an SAPO-34 catalyst.
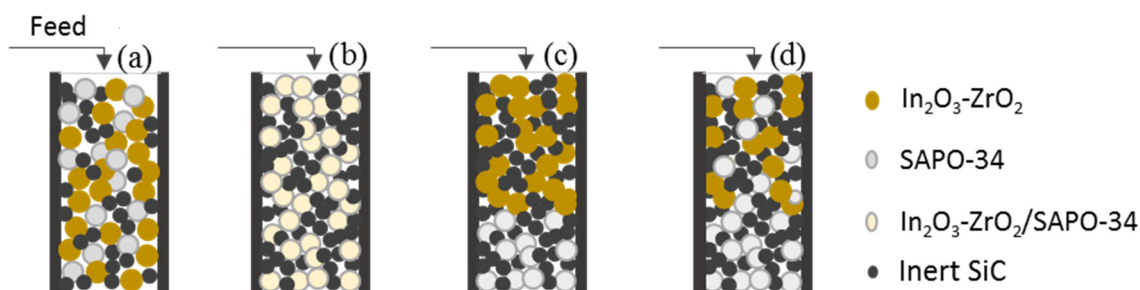
Figure 2. Different configurations of the catalytic bed for the tandem In_2O_3-ZrO_2/SAPO-34 catalysts. (**a**) Physical mixture, (**b**) hybrid catalyst, (**c**) dual bed (In_2O_3-ZrO_2 and subsequent SAPO-34), (**d**) dual bed (In_2O_3-ZrO_2/SAPO-34 in physical mixture and subsequent SAPO-34 bed).

Attending to the results of product-yield evolution with time on stream in Figure 3 (corresponding to an equimolecular CO_2 and CO feed), the differences were noteworthy, and evidenced the great relevance of the configuration of the catalyst/bed for this process. Configuration (a) led to an outstanding olefin yield and great stability of the catalyst (Figure 3a). The results obtained with the hybrid catalyst (Figure 3b) were remarkably lower than those for the former configuration due to the deterioration of the individual catalyst properties with pelletizing. In Section 3.2, the deterioration of the surface properties and acidity in the pelletization is attributed to the partial blocking of the micropores in the SAPO-34 catalyst by In_2O_3-ZrO_2. According to the results in Figure 3c, the dual-bed configuration was not suitable for this process, because, with the separation of the

individual catalysts, no synergy was generated between the reaction mechanisms of the steps of the oxygenates' synthesis and their conversion into olefins, and, consequently, the severe thermodynamic limitations of the first step [36] were not reduced.

Figure 3. Comparison of the evolution of product yields with time on stream for different In_2O_3-ZrO_2/SAPO-34 catalyst and bed configurations. (**a**) In physical mixture, (**b**) hybrid catalyst, (**c**) dual bed (In_2O_3-ZrO_2 and subsequent SAPO-34), (**d**) dual bed (In_2O_3-ZrO_2/SAPO-34 in physical mixture and subsequent SAPO-34 bed). Reaction conditions: feed, H_2/CO/CO_2; 400 °C; 30 bar; H_2/CO_x, 3; CO_2/CO_x, 0.5; space time, 3.35 g_{InZr} h mol_C^{-1}.

Finally, configuration (d) was tested to pursue further improvements to the results obtained with the best configuration, (a), by converting the oxygenates remaining with an additional SAPO-34 bed on-line. However, as observed in Figure 3d, this configuration was unsuccessful. The oxygenate yield was lower and the olefin yield decayed to a third. CO_x conversion was also lower (4.1% and 2.6%) and olefin selectivity was penalized, with paraffins being the main products. The activity of SAPO-34 for olefins' conversion into paraffins can be explained by the presence of strong acid sites, active for hydrogen transfer mechanisms [35]. Moreover, these mechanisms are relevant for olefins' condensation into aromatics and of the latter into polyaromatic coke structures [37], explaining the pronounced initial deactivation which occurred in the first 4 h on stream (Figure 3d). The extent of these undesired reactions decreased with the time on stream due to the deactivation of the strong acid sites of SAPO-34, leading to the decay of the paraffin yield. Hence, the relevance of the deactivation of SAPO-34 in the results and the role of SAPO-34 in paraffin formation from olefins are ratified.

Attending to the aforementioned results, the best performance of the physical mixture of the individual catalysts (configuration (a) in Figure 2) with respect to other tandem catalyst configurations for the direct hydrogenation of CO_2/CO mixtures into olefins is consistent with the results reported by Gao et al. [30] for CO_2 feeds. It should be noted that the results in Figure 1 correspond to 16 h on stream, when the catalyst has reached a pseudo-steady state of almost constant remnant activity. The greater stability of this tandem catalyst is a consequence of the positive synergy of the vicinity of In_2O_3-ZrO_2 and SAPO-34. Thus, the active sites of In_2O_3-ZrO_2 contribute to the hydrogenation of the hydrocarbons' precursors to coke deposition (the oligomers generated from olefins), minimizing the blockage of acid sites and of the cages in the microporous structure of SAPO-34.

2.3. Catalyst Reduction Treatment

XPS analyses were carried out with the methodology described in Section 3.2. The results (Table 1 and Figure S2 in the Supplementary Materials) evidenced that subjecting the catalyst (prepared through physical mixture with an SAPO-34 to In_2O_3-ZrO_2 mass ratio of 1/2) to a H_2 atmosphere prior to reaction influenced the In^0/In_2O_3 ratio. The partial reduction consisted of subjecting the catalyst to 10 cm^3 min^{-1} of H_2 at a partial pressure of 2 bar, at 400 °C for 2 h. This procedure reduced ~4% of the superficial In_2O_3 to In^0, whereas a more severe treatment with a H_2 partial pressure of 15 bar (also at 400 °C for 2 h) completely reduced In_2O_3 (100%) to In^0.

Table 1. In^0/In_2O_3 ratio in the surface of the catalyst subjected to different reduction treatments.

Treatment	In^0/In_2O_3 Ratio
Without treatment	0
Partial reduction	0.04
Complete reduction	Infinite

To ascertain the effect of reduction, the results of the product-yields' evolution with the time on stream of the In_2O_3-ZrO_2/SAPO-34 tandem catalyst without reduction treatment (Figure 4a) were compared with those of a catalyst subjected to partial reduction (Figure 4b). The results correspond to a reaction with H_2/CO feed at 400 °C and 30 bar. As observed, with both catalysts, the yields of olefins and paraffins decreased sharply with time on stream until reaching constant values after 4 h on stream. This non-steady period must be related to the deactivation of the catalyst. Moreover, oxygenates' presence in the product stream indicates that deactivation affects the SAPO-34 catalyst. In addition, the lower activity for olefin formation can explain the formation of methane through the parallel methanation route, activated by the In_2O_3-ZrO_2 catalyst.

Attending to the higher olefin yield achieved in the pseudo-steady state with the partially reduced catalysts (Figure 4b), this reduction contributed remarkably to the performance of the catalyst in a positive way. Thus, hydrocarbon (methane + paraffins + olefins) yield increased over 60%, and olefin yield boosted 50%, from ~ 2% for the catalyst without reduction (without In^0 presence) (Figure 4a) to 3%, which is consistent with the increase in the In^0/In_2O_3 ratio to 0.04.

In Figure S3 (in the Supplementary Materials), the product yields of the catalysts without and with reduction treatments are compared in the pseudo-steady state (conditions after 16 h on stream, Figure 4). The results evidenced the great sensitivity of the active sites in the In_2O_3-ZrO_2 catalyst, in which a partial reduction had a notable effect on activity, boosting CO_x conversion and olefin yield. These findings might be in line with the observation of Tsoukalou et al. [12]. Thus, these authors verified via in operando analyses that partially reducing the In_2O_3 structure to In_2O_{3-x}, with an oxidation state between $^+3$ and $^+2$, results in the better performance of the catalyst in the pseudo-steady state. This result can be explained by the higher activity of the partially reduced catalyst for hydrogenating coke precursors, easing the higher remnant activity of the catalyst in the pseudo-steady state.
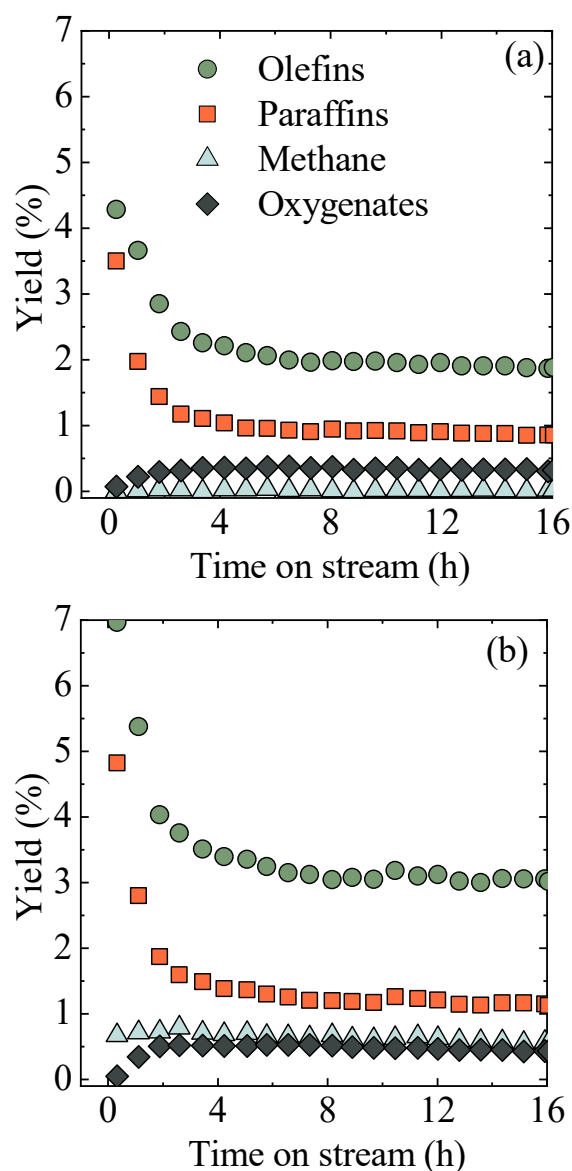
Figure 4. Evolution of product yields with time on stream with catalysts (**a**) without treatment, and (**b**) subjected to partial reduction with H_2. Reaction conditions: feed, H_2/CO; 400 °C; 30 bar; H_2/CO_x ratio, 3; CO_2/CO_x, 0; space time, 3.35 g_{InZr} h mol_C^{-1}.

To assess the joint effect of the feed composition and catalyst reduction intensity, the results in Figure 5 (for the hydrogenation of an equimolecular CO_2 and CO mixture) correspond to the catalyst without reduction treatments (Figure 5a), and that subjected to partial (Figure 5b) and complete reduction (Figure 5c). The reaction conditions were similar to those in Figure 4 and Figure S3 (in the Supplementary Materials) (for a CO feed). Comparing the results in Figure 5a,b with those in Figure 4a,b, respectively, a lower initial deactivation rate was observed with the co-feeding of CO_2. This effect is attributable to the higher H_2O concentration in the medium, which was formed mainly by the reverse water–gas shift (rWGS) reaction (Equation (5)). The role of H_2O in attenuating coke deactivation in this reaction was already proven and it is related to the decrease in the extent of condensation reactions of coke precursors into polyaromatic structures that remain retained in the micropores and block the acid active sites of SAPO-34 [38]. This effect of H_2O on attenuating coke deposition is general in acid [39] and bifunctional [40] catalysts.
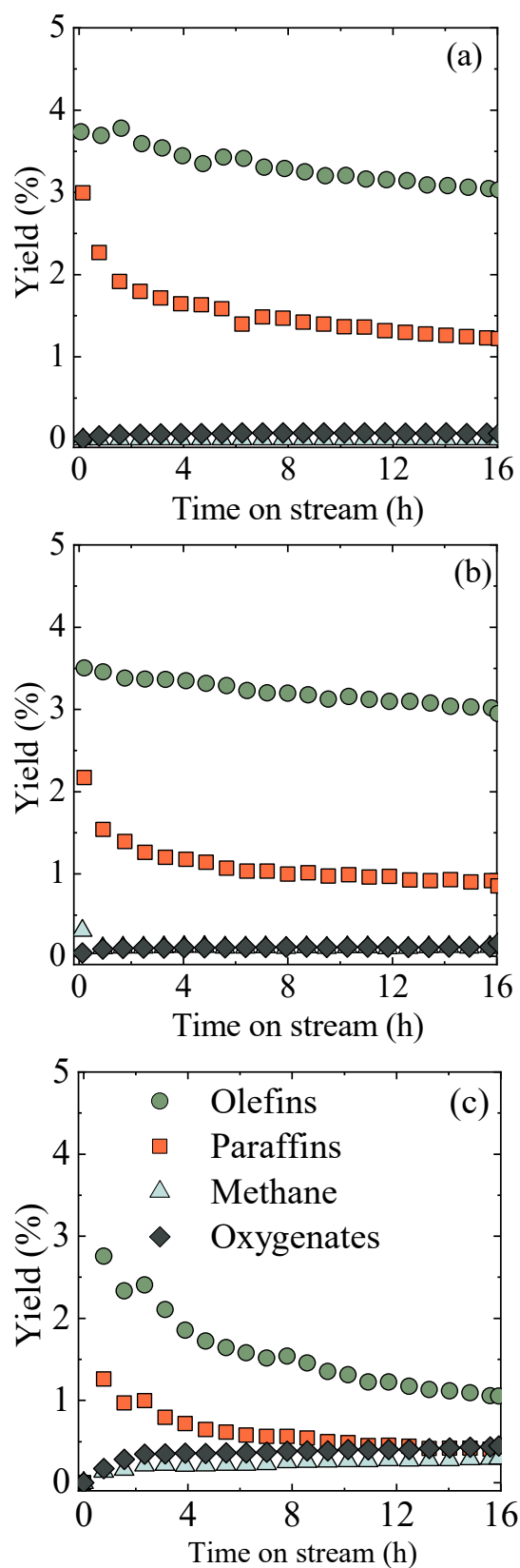
Figure 5. Evolution of product yields with time on stream with catalysts: (**a**) without reduction, (**b**) subjected to partial reduction, (**c**) subjected to complete reduction. Reaction conditions: feed, $H_2/CO_2/CO$; 400 °C; 30 bar; H_2/CO_x, 3; CO_2/CO_x, 0.5; space time, 3.35 g_{InZr} h mol_C^{-1}.

The different apparent effect of the reduction of the catalyst on the results at zero time on stream (fresh catalyst) and for the pseudo-steady state of the catalyst (partially deactivated by coke) is also observed in Figure 5. Thus, it was detected that after a partial reduction (Figure 5b), the initial activity of the catalyst for olefin production and the initial yield of paraffins (product of olefin hydrogenation) were slightly lower than for the catalyst without reduction (Figure 5a). The decrease in the capacity to hydrogenate olefins was also significant with the partially reduced catalyst, which resulted in a lower paraffin yield. In Figure 5c, corresponding to the catalyst with a complete reduction of In_2O_3 to In^0, the reported trend of reduction on the initial yield of olefins is accentuated. A continued decay with time on stream in the olefins' formation reaction rate and their hydrogenation is also observed in Figure 5c, with the presence of oxygenates and CH_4 in the product stream, evidencing the activity of In^0 sites for methanation.

In Figure S4 (in the Supplementary Materials), the results (product yields and CO_2 and CO_x conversion) at 16 h on stream (pseudo-steady state of the catalysts) for the three catalysts are compared. As observed, the partial H_2 reduction treatment led to the increased CO_2 conversion, slightly decreasing the conversion of CO_x with respect to the catalyst without reduction, which is explained by the higher formation of CO via the rWGS reaction (Equation (5)). The lower paraffin yield than for the catalyst without reduction indicates a decrease in the hydrogenation activity of the catalysts, to which the increase in H_2O concentration (product of the rWGS reaction) will contribute. Thus, although the olefins' yield decreased slightly with the partial reduction, their selectivity increased (from <70% for the catalyst without the treatment of partial reduction to 72.5%). However, the catalyst subjected to a complete reduction of In_2O_3 (Figure 5c) gave way to poor hydrocarbon yield and lower CO_2 and CO_x conversion values due to the lower presence of active sites (oxygen vacancies) in the catalyst. A higher yield of methane was also observed with this catalyst (Figure S4, in the Supplementary Materials).

Attending to the aforementioned results regarding the sensitivity of the In_2O_3-ZrO_2/SAPO-34 tandem catalyst to the reduction prior to reaction, and to the importance of catalyst deactivation to explain its performance in the pseudo-steady state, it must be pointed out that these results also depend on the CO and CO_2 content in the feed. Thus, while in the hydrogenation of CO a partial reduction had a favorable effect on the yield of olefins and on catalyst activity in the pseudo-steady state, for the hydrogenation of a CO_2/CO mixture, the partial reduction barely had any effect. The difference may be attributed to the role of the concentration of H_2O in attenuating coke deposition on the SAPO-34 catalyst in the conversion of oxygenates [41,42]. The presence of CO_2 in the feed favors the formation of H_2O through the rWGS reaction (Equation (4)), partially fading the effect of the catalyst reduction. On the contrary, for the hydrogenation of CO and CO_2/CO mixtures, a more severe reduction treatment had a negative incidence over catalyst activity in the pseudo-steady state as a consequence of the lessening of oxygen vacancies (diminishing the activity for methanol synthesis and for the hydrogenation of coke precursors in the SAPO-34) and selectivity (since methanation was favored).

In a previous work [31], the deactivation of the In_2O_3-ZrO_2/SAPO-34 catalyst was studied in detail under the reaction conditions used in this study. The results were of significant relevance to establish the optimal conditions for the process and for the configuration of the catalyst. Coke deposition was identified as the cause for catalyst deactivation, which mainly occurs in the SAPO-34, and barely in the In_2O_3-ZrO_2 catalyst. In addition, the coke deposition phenomenon is complex, given that it is affected by the concentration of H_2O (attenuating coke deposition) and oxygenates (methanol/dimethyl ether), given their role as coke precursors. Moreover, deactivation is also attenuated by the high partial pressure of H_2. In such an atmosphere, the In_2O_3-ZrO_2 catalyst plays a key role in activating the hydrogenation reactions of coke precursor intermediates, thus attenuating deactivation. It is noteworthy that the balance between coke deposition and removal in the catalyst allows a pseudo-steady state of significant remnant activity to be reached, as confirmed in the aforementioned results of this manuscript. Given the relevance of deactivation for the

viability and scale-up of the process, it is an aspect that requires further attention in order to develop new stable catalysts with an appropriate configuration.

3. Materials and Methods

3.1. Catalyst Preparation

In_2O_3-ZrO_2 catalyst was synthesized via co-precipitation of $In(NO_3)_3$ (Sigma-Aldrich, St. Louis, MO, USA) and $Zr(NO_3)_4$ (Panreac) (1M) in an In/Zr atomic ratio of 2 with ammonium carbonate (Panreac, 1 M) at 70 °C and neutral pH, as described in detail in a previous work [19]. The mixture was aged for 2 h, filtered, washed with deionized water, dried and calcined at 500 °C for 1 h. The resulting powder was pelletized, crushed and sieved to obtain 125–400 μm particle size. As acid catalyst, a commercial SAPO-34 molecular sieve (ACS Material, Pasadena, CA, USA) was used. The provided powder was calcined at 500 °C for 1 h and pelletized into 125–400 μm particles.

The In_2O_3-ZrO_2/SAPO-34 catalyst was prepared and used with the following configuration (Figure 2): (i) physical mixture of SAPO-34 and In_2O_3-ZrO_2 catalysts (individually pelletized as aforementioned) in a mass ratio within the 0 to 6 range; (ii) hybrid catalyst, prepared via mixing and powdering SAPO-34 and In_2O_3-ZrO_2 (in a 1/2 mass ratio) in a mortar until a homogeneous mixture was obtained, and subsequent joint pelletizing in the 125–400 μm range; (iii) sequential arrangement of two catalyst beds, placing first the In_2O_3-ZrO_2 catalyst for the hydrogenation of CO_2/CO and, subsequently, the SAPO-34 catalyst for the on-line conversion of the oxygenates into hydrocarbons; (iv) likewise, two catalytic beds in tandem, placing first a physical mixture of SAPO-34 and In_2O_3-ZrO_2 with a 1/2 mass ratio (as in the hybrid catalyst) and, subsequently, an additional SAPO-34 catalyst bed, pursuing the conversion of the possible remaining oxygenates.

3.2. Catalyst Characterization

The textural properties of the catalysts, thus, pore distribution, pore volume and BET specific surface area, were determined using N_2 adsorption–desorption analyses in Micromeritics ASAP 2010 equipment (Norcross, CA, USA) at cryogenic liquid N_2 temperature (−196 °C). Prior to the analysis, the samples were subjected to 10^{-3} mm Hg vacuum at 150 °C under He atmosphere for 8 h to remove possibly adsorbed impurities and H_2O. The resulting isotherms and the pore distribution, determined using the Barrett–Joyner–Halenda (BJH) method and applied to the adsorption branch of the isotherm, are shown in Figure 6. For the In_2O_3-ZrO_2 catalyst, a hysteresis typical of mesoporous materials is observed in Figure 1a at relative pressures over 0.6, whereas for the SAPO-34 catalyst, an exclusive microporous nature is observed. The isotherm of the hybrid catalyst (mortar-mixed and subsequently pelletized) showed lower microporosity than expected from the combination of In_2O_3-ZrO_2 and SAPO-34 catalysts. In fact, the BET surface area of 98 m^2 g^{-1} and micropore volume of 0.03 cm^3 g^{-1} of the hybrid catalyst in Table 2 is not in accordance with the In_2O_3-ZrO_2/SAPO-34 ratio, indicating that further interactions among both catalysts took place. As observed in Figure 6b and Table 2, the hybrid catalyst was barely more microporous than the In_2O_3-ZrO_2 catalyst (with significant pore volume), evidencing that a large amount of the micropores of the SAPO-34 catalyst were blocked during the pelletizing of both catalyst powders. Consequently, the pore volume of the In_2O_3-ZrO_2/SAPO-34 hybrid catalyst was 0.13 cm^3 g^{-1}, due to the presence of mesopores of In_2O_3-ZrO_2, although the blockage of these in the pelletizing stage was also remarkable. Likewise, the average diameter of the pores of the hybrid catalyst (32 Å) is a consequence of the contribution of In_2O_3-ZrO_2 catalyst mesopores, the size of which reduced in the pelletizing stage. The average pore diameters follow the expected order: In_2O_3-ZrO_2 > Hybrid > SAPO-34.
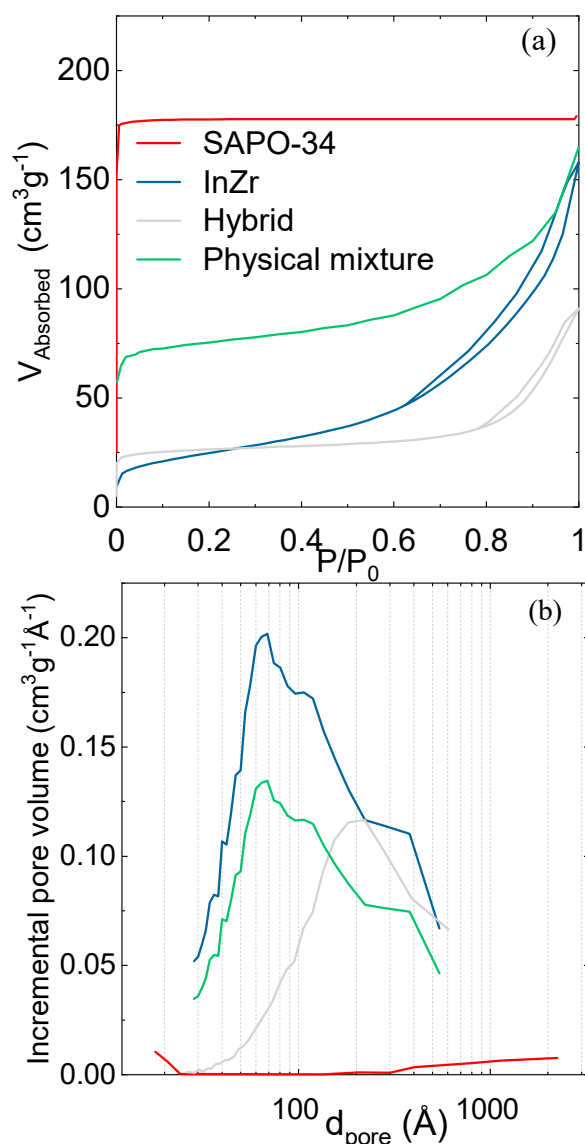
Figure 6. N_2 adsorption-desorption isotherms (**a**) and pore-volume distribution (**b**) of the catalysts.

Table 2. Textural properties of the catalysts.

Catalyst	S_{BET} (m^2 g^{-1})	$V_{micropore}$ (cm^3 g^{-1})	V_{pore} (cm^3 g^{-1})	d_p (Å)
In_2O_3-ZrO_2	86	-	0.23	90
SAPO-34	652	0.22	0.23	15
Hybrid In_2O_3-ZrO_2/SAPO-34	98	0.03	0.13	32

H_2 and CO temperature-programed reduction (H_2-TPR and CO-TPR, respectively), and temperature-programed CO_2 desorption (CO_2-TPD) were carried out in Micromeritics Autochem 2920 equipment (Norcross, CA; USA), following the procedure described in previous works [19,43]. Briefly, for the TPR assays (gathered in Figure S6 in the Supplementary Materials), 100 mg of sample was subjected to a sweeping with He (200 °C, 60 min) to eliminate impurities and absorbed H_2O and heated up to 800 °C at 2 °C min^{-1} rate in H_2 or CO atmosphere (10% H_2 or CO, diluted in Ar). For the CO_2-TPD (Figure S7 in the Supplementary Materials), the sweeping treatment was carried out at 550 °C (for 30 min), and after stabilization and saturation of the sample with CO_2 injections at 50 °C, the physically retained adsorbate was swept with He. The desorption of the chemically

adsorbed CO_2 was carried out by heating the sample at a 5 °C min^{-1} rate from 50 to 400 °C. Scanning Electron Microscopy was carried out to analyze the catalyst samples (Figure S5 in the Supplementary Materials). Figure S5 (in the Supplementary Materials) shows the characteristic cubic crystals of the SAPO-34 sample [44] and the In_2O_3-ZrO_2 particles, the latter being characteristic of polyhedrons with smaller particle sizes [34]. SAPO-34 cubic samples of the hybrid catalysts appear chipped and cracked as a consequence of the pelletization step, as also observed for other bifunctional catalysts, since the metallic oxides partially blocked the micropores [45].

The TPR analyses (Figure S6 in the Supplementary Materials) evidenced the higher reduction capacity of CO than of H_2 (related to the splitting activity), which is in accordance with other studies on the In_2O_3 catalysts [17,18,46,47]. From the CO_2-TPD analyses (Figure S7, in the Supplementary Materials), the CO_2 adsorption capacity of In_2O_3-ZrO_2 catalysts was ascertained to be higher than that of the parent In_2O_3 and ZrO_2 catalysts [19]. From these assays, the effect of CO as vacancy generator was also determined in the literature [13,17,19], which will favor CO and CO_2 adsorption, and, thus, will contribute to upturning the production of light olefins.

To determine the reduction state of the In in the In_2O_3-ZrO_2 catalyst, XPS analyses were carried out using a SPECS system equipped with a Phoibos 150 1D-DLD analyzer (SpecsGroup, Berlin, Germany) and a monochromic Al-Kα radiation source. Prior to the analysis, the spectrometer was calibrated with Ag (Ag 3d^5/2368.26 eV) and the samples were outgassed. An initial scan was carried out using a step energy of 1 eV, dwell time of 0.1 s and a pass energy of 80 eV followed by a detailed scan using a step energy of 1 eV, dwell time of 0.1 s and a pass energy of 30 eV. CasaXPS 2.3.16 software was used to fit the spectra according to Gaussian–Lorentzian model. Each analysis was repeated three times to ensure the results. The results are listed in Table 1 and the XPS profiles are plotted in Figure S2 in the Supplementary Materials.

As previously mentioned, the partial reduction consisted of treatment with H_2 (10 cm^3 min^{-1}) at a partial pressure of 2 bar and 400 °C for 2 h. According to the results in Table 1, this procedure reduced ~4% of the superficial In_2O_3 to In^0, whereas the treatment with a H_2 partial pressure of 15 bar (also at 400 °C for 2 h) completely reduced In_2O_3 (100%) to In^0.

The acidity was determined using NH_3 temperature-programmed desorption (NH_3-TPD, Figure S8 in the Supplementary Materials) in Micromeritics Autochem 2920 equipment (Norcross, CA, USA). NH_3 injections were conducted at 150 °C until the complete saturation of the sample, and the desorption was carried out at a 5 °C min^{-1} temperature rate up to 550 °C. The results listed in Table 3 evidence the higher acidity of the SAPO-34 catalyst compared with In_2O_3-ZrO_2. The hybrid catalyst presents an intermediate acidity (319 μmol_{NH3} g_{cat}^{-1}) lower than the weighted average of In_2O_3-ZrO_2 and zeolite catalysts (340 μmol_{NH3} g_{cat}^{-1}), indicating that a partial blockage of the acid sites of SAPO-34 catalyst occurred during the pelletizing step of the preparation of the hybrid catalyst (as observed in Table 2 and Figure S8 (in the Supplementary Materials)). Comparing the NH_3-TPD profiles of the catalysts prepared via pelletization (hybrid) and physical mixing, a noticeable decrease in the amount of strong acid sites was observed in the former for the SAPO-34 catalyst, particularly for the sites where NH_3 desorbed above 325 ºC. In contrast, the amount of acid sites in SAPO-34 remained unaffected with the physical mixing. This effect of pelletization, deteriorating the acidity of SAPO-34, is consistent with the aforementioned degradation of the porous structure (Table 2) and justifies the negative synergy observed due to pelletization when comparing the behavior of the two tandem catalysts in Figure 3 (Section 2.2).

Table 3. Acidity of the catalysts (in $\mu mol_{NH3}\ g_{cat}^{-1}$).

In_2O_3-ZrO_2	123
SAPO-34	778
Hybrid In_2O_3-ZrO_2/SAPO-34	319

3.3. Reaction and Analysis Equipment

The reaction experiments were carried out in PID Eng & Tech Microactivity Reference automated equipment (PID Eng.&Tech., Madrid, Spain), described elsewhere [43], provided with an isothermal 316 stainless steel reactor. The scheme of the equipment is depicted in Figure S9 (in the Supplementary Materials). Whatever the catalyst configuration, the catalytic packed bed is composed of catalyst diluted in SiC (0.035 mm particle size), an inert solid, to ascertain isothermal conditions, avoid preferential paths and ensure a suitable bed height when operating at small space-time values.

For the analysis of the feed and product stream, a Varian CP-4900 (CA, USA) micro chromatograph equipped with three different chromatographic columns was used: (i) Porapak Q (PPQ) (10 m $\times$ 20 μm) for quantifying CO_2, methane, H_2O, C_2-C_4 hydrocarbons, methanol and dimethyl ether; (ii) molecular sieve (MS-5) (10 m $\times$ 12 μm) for quantifying H_2, N_2, O_2 and CO; and (iii) 5 CB column (CPSiL) (8 m $\times$ 2μm) for quantifying C_{4+} hydrocarbons. Periodically, the micro-GC was calibrated with standards of known composition.

The reaction runs were typically carried out at 400 °C; 30 bar; space time (referred to as In_2O_3-ZrO_2 catalyst mass in the bed; H_2/(CO_x) ratio in the feed, 3; CO_2/(CO_x) ratios in the feed of 0 (H_2/CO), 0.5 (H_2/CO/CO_2) and 1 (H_2/CO_2); time on stream (TOS) up to 16 h; and 3.35 g_{InZr} h mol_C^{-1}. The space-time value corresponded to 1.22 10^{-1} g of InZr catalyst mass and a molar flow rate of 3.68 10^{-2} mol CO_2/CO h^{-1}. It should be noted that these reaction conditions were established in a previous work as adequate for promoting olefin selectivity in the joint conversion of CO_2 and syngas [19]. The temperature (400 °C) and pressure (30 bar) were intermediate to the optimal values for each of the integrated reaction stages (synthesis of methanol and its conversion into olefins), which allowed us to reach a good compromise of the extent of both reactions. The low space-time value guaranteed gathering results in kinetic regime with deactivation of the catalyst, which allowed us to clearly evaluate the effect of the feed composition and catalyst configurations. As regards the H_2/CO_x mol ratio, a value between 2 and 3 is suggested to maximize olefin yield, olefin/paraffin ratio and CO_x conversion, since higher H_2 content, besides its higher cost, does not lead to improvements in the results.

3.4. Reaction Indices

The results were quantified according to conversion, product yield and selectivity in content C unit basis. The conversion of CO_x was defined as:

$$X_{CO_x} = \frac{F^0_{CO_x} - F_{CO_x}}{F^0_{CO_x}} \cdot 100 \tag{6}$$

and that of the CO_2 analogously:

$$X_{CO_2} = \frac{F^0_{CO_2} - F_{CO_2}}{F^0_{CO_2}} \cdot 100 \tag{7}$$

where $F^0_{CO_x}$ and F_{CO_x} are the CO_x molar flow rates at the inlet and outlet of the reactor, respectively, and $F^0_{CO_2}$ and F_{CO_2} are the corresponding rates for CO_2.

Yield and selectivity (Y_i and S_i, respectively) were determined for the following lumps: C_2–C_4 olefins, C_2–C_4 paraffins, methane and oxygenates (methanol and DME):

$$Y_i = \frac{n_i \cdot F_i}{F_{CO_x}^0} \cdot 100 \qquad (8)$$

$$S_i = \frac{n_i \cdot F_i}{\sum_i (n_i \cdot F_i)} \cdot 100 \qquad (9)$$

where n_i is the number of C atoms in a molecule of each compound i and F_i is the corresponding molar flow rate at the reactor outlet stream.

To guarantee the reliability of the results, the reaction indices in this work are mean values obtained in three experiments, with deviations lower than 5%.

4. Conclusions

The performance of the In_2O_3-ZrO_2/SAPO-34 tandem catalyst in the hydrogenation of CO_2/CO mixtures into olefins is highly sensitive (in yield, selectivity and stability) to the composition (SAPO-34 to In_2O_3-ZrO_2 mass ratio), catalyst configuration (hybrid or mixture of individual catalysts) and intensity of the catalysts' reduction. The prompt deactivation of the catalyst (due to coke deposition on the SAPO-34 catalyst) conditions the results and, therefore, the interest should focus on the performance of the catalyst once acquired a pseudo-steady state of almost constant activity.

As for the configuration of the tandem catalyst, the physical mixture with an SAPO-34 to In_2O_3-ZrO_2 mass ratio of 0.5 was ascertained as optimal for all the tested compositions (CO_2/CO_x ratio from 0 to 1) attending to the results in the pseudo-steady state of the catalyst. It should be noted that the further addition of SAPO-34 entails olefins' hydrogenation into paraffins. The preparation of the hybrid catalyst through pelletizing led to the partial blockage of the SAPO-34 pores, diminishing the oxygenate conversion capacity and hampering the synergy between the reaction mechanisms over both catalysts.

Moreover, the interest in the previous partial reduction of the tandem catalyst depends on the feed composition (CO_2/CO ratio). For CO hydrogenation, partially reducing the catalyst resulted in higher olefin yields and selectivity in the pseudo-steady state of the catalyst, since the activity for the rWGS reaction was favored, forming H_2O and attenuating the deactivation by coke. However, the reduction period is critical, as an over-reduction of the In_2O_3 in the catalyst leads to penalizing its selectivity to methanol/DME production, lessening the activity for the hydrogenation of coke precursors and promoting methanation. For the joint hydrogenation of CO_2 and CO mixtures (with higher concentrations of H_2O), the partial reduction (corresponding to a superficial In^0/In_2O_3 ratio of 0.04) of the catalyst had a favorable effect, but to a lower extent than for CO hydrogenation.

Supplementary Materials: The following supporting information can be downloaded at: https://www.mdpi.com/article/10.3390/catal13071101/s1, Figure S1: Effect of SAPO-34/In_2O_3-ZrO_2 mass ratio in the tandem catalyst on products yields. Feed: (a) H_2/CO/CO_2, (b) H_2/CO_2. Reaction conditions: 400 °C; 30 bar; H_2/CO_x, 3; space time, 3.35 gInZr h molC^{-1}; time on stream, 16 h; Figure S2: XPS profiles of In_2O_3-ZrO_2 catalyst subjected to different reduction treatments: (a) without treatment, (b) partial reduction, (c) complete reduction; Figure S3: Effect of catalyst reduction on products yields and on COx conversion. Reaction conditions: feed, H_2/CO; 400 °C; 30 bar; H_2/CO_x ratio, 3; CO_2/CO_x, 0; space time, 3.35 gInZr h molC^{-1}; time on stream, 16 h; Figure S4: Effect of catalyst treatment on product yields and COx and CO_2 conversion. Reaction conditions: feed, H_2/CO_2/CO; 400 °C; 30 bar; H_2/CO_x, 3; CO_2/CO_x, 0.5; space time, 3.35 gInZr h molC^{-1}; time on stream, 16 h; Figure S5: SEM image of the hybrid In_2O_3-ZrO_2/SAPO-34 catalyst; Figure S6: H_2-TPR and CO-TPR profiles for In_2O_3-ZrO_2 catalyst; Figure S7: CO_2-TPD profile for In_2O_3-ZrO_2 catalyst; Figure S8: NH_3-TPD profiles for the In_2O_3-ZrO_2, SAPO-34, hybrid In_2O_3-ZrO_2/SAPO-34 catalyst and In_2O_3-ZrO_2/SAPO-34 prepared by physical mixture of both; Description of the reaction equipment; Figure S9: Flow diagram of the reaction equipment.

Data Availability Statement: Data is contained within the article or Supplementary Materials.

Conflicts of Interest: The authors declare no conflict of interest.

References

1. International Energy Agency. Net Zero by 2050—Analysis—IEA. Available online: https://www.iea.org/reports/world-energy-outlook-2021 (accessed on 2 July 2023).
2. Cordero-Lanzac, T.; Ramirez, A.; Navajas, A.; Gevers, L.; Brunialti, S.; Gandía, L.M.; Aguayo, A.T.; Sarathy, S.M.; Gascon, J. A Techno-Economic and Life Cycle Assessment for the Production of Green Methanol from CO_2: Catalyst and Process Bottlenecks. *J. Energy Chem.* **2022**, *68*, 255–266. [CrossRef]
3. Alabdullah, M.A.; Gomez, A.R.; Vittenet, J.; Bendjeriou-Sedjerari, A.; Xu, W.; Abba, I.A.; Gascon, J. A Viewpoint on the Refinery of the Future: Catalyst and Process Challenges. *ACS Catal.* **2020**, *10*, 8131–8140. [CrossRef]
4. Gholami, Z.; Gholami, F.; Tišler, Z.; Vakili, M. A Review on the Production of Light Olefins Using Steam Cracking of Hydrocarbons. *Energies* **2021**, *14*, 8190. [CrossRef]
5. Gholami, Z.; Gholami, F.; Tišler, Z.; Tomas, M.; Vakili, M. A Review on Production of Light Olefins via Fluid Catalytic Cracking. *Energies* **2021**, *14*, 1089. [CrossRef]
6. Tian, P.; Wei, Y.; Ye, M.; Liu, Z. Methanol to Olefins (MTO): From Fundamentals to Commercialization. *ACS Catal.* **2015**, *5*, 1922–1938. [CrossRef]
7. Pawelec, B.; Guil-López, R.; Mota, N.; Fierro, J.L.G.; Yerga, R.M.N. Catalysts for the Conversion of CO_2 to Low Molecular Weight Olefins—A Review. *Materials* **2021**, *14*, 6952. [CrossRef] [PubMed]
8. Orege, J.I.; Liu, N.; Amoo, C.C.; Wei, J.; Ge, Q.; Sun, J. Boosting CO_2 Hydrogenation to High-Value Olefins with Highly Stable Performance over Ba and Na Co-Modified Fe Catalyst. *J. Energy Chem.* **2023**, *80*, 614–624. [CrossRef]
9. Guo, S.; Wang, H.; Qin, Z.; Li, Z.; Wang, G.; Dong, M.; Fan, W.; Wang, J. Feasibility, Limit, and Suitable Reaction Conditions for the Production of Alcohols and Hydrocarbons from CO and CO_2 through Hydrogenation, a Thermodynamic Consideration. *Ind. Eng. Chem. Res.* **2022**, *61*, 17027–17038. [CrossRef]
10. Liu, X.; Zhou, W.; Yang, Y.; Cheng, K.; Kang, J.; Zhang, L.; Zhang, G.; Min, X.; Zhang, Q.; Wang, Y. Design of Efficient Bifunctional Catalysts for Direct Conversion of Syngas into Lower Olefins via Methanol/Dimethyl Ether Intermediates. *Chem. Sci.* **2018**, *9*, 4708–4718. [CrossRef]
11. Al-Qadri, A.A.; Nasser, G.A.; Adamu, H.; Muraza, O.; Saleh, T.A. CO_2 Utilization in Syngas Conversion to Dimethyl Ether and Aromatics: Roles and Challenges of Zeolites-Based Catalysts. *J. Energy Chem.* **2023**, *79*, 418–449. [CrossRef]
12. Tsoukalou, A.; Abdala, P.M.; Stoian, D.; Huang, X.; Willinger, M.G.; Fedorov, A.; Müller, C.R. Structural Evolution and Dynamics of an In_2O_3 Catalyst for CO_2 Hydrogenation to Methanol: An Operando XAS-XRD and in Situ TEM Study. *J. Am. Chem. Soc.* **2019**, *141*, 13497–13505. [CrossRef]
13. Wang, J.; Zhang, G.; Zhu, J.; Zhang, X.; Ding, F.; Zhang, A.; Guo, X.; Song, C. CO_2 Hydrogenation to Methanol over In_2O_3-Based Catalysts: From Mechanism to Catalyst Development. *ACS Catal.* **2021**, *11*, 1406–1423. [CrossRef]
14. Ye, J.; Liu, C.; Ge, Q. DFT Study of CO_2 Adsorption and Hydrogenation on the In_2O_3 Surface. *J. Phys. Chem. C* **2012**, *116*, 7817–7825. [CrossRef]
15. Ye, J.; Liu, C.; Mei, D.; Ge, Q. Active Oxygen Vacancy Site for Methanol Synthesis from CO_2 Hydrogenation on In_2O_3 (110): A DFT Study. *ACS Catal.* **2013**, *3*, 1296–1306. [CrossRef]
16. Sun, K.; Fan, Z.; Ye, J.; Yan, J.; Ge, Q.; Li, Y.; He, W.; Yang, W.; Liu, C.-j. Hydrogenation of CO_2 to Methanol over In_2O_3 Catalyst. *J. CO_2 Util.* **2015**, *12*, 1–6. [CrossRef]
17. Martin, O.; Martín, A.J.; Mondelli, C.; Mitchell, S.; Segawa, T.F.; Hauert, R.; Drouilly, C.; Curulla-Ferré, D.; Pérez-Ramírez, J. Indium Oxide as a Superior Catalyst for Methanol Synthesis by CO_2 Hydrogenation. *Angew. Chemie* **2016**, *128*, 6369–6373. [CrossRef]
18. Dang, S.; Gao, P.; Liu, Z.; Chen, X.; Yang, C.; Wang, H.; Zhong, L.; Li, S.; Sun, Y. Role of Zirconium in Direct CO_2 Hydrogenation to Lower Olefins on Oxide/Zeolite Bifunctional Catalysts. *J. Catal.* **2018**, *364*, 382–393. [CrossRef]

19. Portillo, A.; Ateka, A.; Ereña, J.; Bilbao, J.; Aguayo, A.T. Role of Zr Loading into In_2O_3 Catalysts for the Direct Conversion of CO_2/CO Mixtures into Light Olefins. *J. Environ. Manag.* **2022**, *316*, 115329. [CrossRef]

20. Numpilai, T.; Wattanakit, C.; Chareonpanich, M.; Limtrakul, J.; Witoon, T. Optimization of Synthesis Condition for CO_2 Hydrogenation to Light Olefins over In_2O_3 Admixed with SAPO-34. *Energy Convers. Manag.* **2019**, *180*, 511–523. [CrossRef]

21. Araújo, T.P.; Shah, A.; Mondelli, C.; Stewart, J.A.; Ferré, D.C.; Pérez-Ramírez, J. Impact of Hybrid CO_2-CO Feeds on Methanol Synthesis over In_2O_3-Based Catalysts. *Appl. Catal. B Environ.* **2021**, *285*, 119878. [CrossRef]

22. Zhou, W.; Cheng, K.; Kang, J.; Zhou, C.; Subramanian, V.; Zhang, Q.; Wang, Y. New Horizon in C1 Chemistry: Breaking the Selectivity Limitation in Transformation of Syngas and Hydrogenation of CO_2 into Hydrocarbon Chemicals and Fuels. *Chem. Soc. Rev.* **2019**, *48*, 3193–3228. [CrossRef]

23. Cai, D.; Cai, Y.; Tan, K.B.; Zhan, G. Recent Advances of Indium Oxide-Based Catalysts for CO_2 Hydrogenation to Methanol: Experimental and Theoretical. *Materials* **2023**, *16*, 2803. [CrossRef] [PubMed]

24. Dang, S.; Li, S.; Yang, C.; Chen, X.; Li, X.; Zhong, L.; Gao, P.; Sun, Y. Selective Transformation of CO_2 and H_2 into Lower Olefins over In_2O_3-ZnZrO$_x$/SAPO-34 Bifunctional Catalysts. *ChemSusChem* **2019**, *12*, 3582–3591. [CrossRef] [PubMed]

25. Martín, N.; Portillo, A.; Ateka, A.; Cirujano, F.G.; Oar-Arteta, L.; Aguayo, A.T.; Dusselier, M. MOF-Derived/Zeolite Hybrid Catalyst for the Production of Light Olefins from CO_2. *ChemCatChem* **2020**, *12*, 5750–5758. [CrossRef]

26. Portillo, A.; Ateka, A.; Ereña, J.; Bilbao, J.; Aguayo, A.T. Alternative Acid Catalysts for the Stable and Selective Direct Conversion of CO_2/CO Mixtures into Light Olefins. *Fuel Process. Technol.* **2022**, *238*, 107513. [CrossRef]

27. Hemelsoet, K.; Van Der Mynsbrugge, J.; De Wispelaere, K.; Waroquier, M.; Van Speybroeck, V. Unraveling the Reaction Mechanisms Governing Methanol-to-Olefins Catalysis by Theory and Experiment. *ChemPhysChem* **2013**, *14*, 1526–1545. [CrossRef]

28. Bjørgen, M.; Svelle, S.; Joensen, F.; Nerlov, J.; Kolboe, S.; Bonino, F.; Palumbo, L.; Bordiga, S.; Olsbye, U. Conversion of Methanol to Hydrocarbons over Zeolite H-ZSM-5: On the Origin of the Olefinic Species. *J. Catal.* **2007**, *249*, 195–207. [CrossRef]

29. Gao, J.; Jia, C.; Liu, B. Direct and Selective Hydrogenation of CO_2 to Ethylene and Propene by Bifunctional Catalysts. *Catal. Sci. Technol.* **2017**, *7*, 5602–5607. [CrossRef]

30. Gao, P.; Dang, S.; Li, S.; Bu, X.; Liu, Z.; Qiu, M.; Yang, C.; Wang, H.; Zhong, L.; Han, Y.; et al. Direct Production of Lower Olefins from CO_2 Conversion via Bifunctional Catalysis. *ACS Catal.* **2018**, *8*, 571–578. [CrossRef]

31. Portillo, A.; Parra, O.; Ereña, J.; Aguayo, A.T.; Bilbao, J.; Ateka, A. Effect of Water and Methanol Concentration in the Feed on the Deactivation of In_2O_3-ZrO$_2$/SAPO-34 Catalyst in the Conversion of CO_2/CO to Olefins by Hydrogenation. *Fuel* **2023**, *346*, 128298. [CrossRef]

32. Gao, P.; Li, S.; Bu, X.; Dang, S.; Liu, Z.; Wang, H.; Zhong, L.; Qiu, M.; Yang, C.; Cai, J.; et al. Direct Conversion of CO_2 into Liquid Fuels with High Selectivity over a Bifunctional Catalyst. *Nat. Chem.* **2017**, *9*, 1019–1024. [CrossRef]

33. Han, Z.; Tang, C.; Wang, J.; Li, L.; Li, C. Atomically Dispersed Ptn+ Species as Highly Active Sites in Pt/In_2O_3 Catalysts for Methanol Synthesis from CO_2 Hydrogenation. *J. Catal.* **2021**, *394*, 236–244. [CrossRef]

34. Wang, J.; Zhang, A.; Jiang, X.; Song, C.; Guo, X. Highly Selective Conversion of CO_2 to Lower Hydrocarbons (C_2-C_4) over Bifunctional Catalysts Composed of In_2O_3-ZrO$_2$ and Zeolite. *J. CO_2 Util.* **2018**, *27*, 81–88. [CrossRef]

35. Li, G.; Jiao, F.; Pan, X.; Li, N.; Miao, D.; Li, L.; Bao, X. Role of SAPO-18 Acidity in Direct Syngas Conversion to Light Olefins. *ACS Catal.* **2020**, *10*, 12370–12375. [CrossRef]

36. Ateka, A.; Pérez-Uriarte, P.; Gamero, M.; Ereña, J.; Aguayo, A.T.; Bilbao, J. A Comparative Thermodynamic Study on the CO_2 Conversion in the Synthesis of Methanol and of DME. *Energy* **2017**, *120*, 796–804. [CrossRef]

37. Qi, L.; Li, J.; Wang, L.; Wang, C.; Xu, L.; Liu, Z. Comparative Investigation of the Deactivation Behaviors over HZSM-5 and HSAPO-34 Catalysts during Low-Temperature Methanol Conversion. *Catal. Sci. Technol.* **2017**, *7*, 2022–2031. [CrossRef]

38. Aguayo, A.T.; del Campo, A.E.S.; Gayubo, A.G.; Tarrío, A.; Bilbao, J. Deactivation by Coke of a Catalyst Based on a SAPO-34 in the Transformation of Methanol into Olefins. *J. Chem. Technol. Biotechnol.* **1999**, *74*, 315–321. [CrossRef]

39. Pérez-Uriarte, P.; Ateka, A.; Gamero, M.; Aguayo, A.T.; Bilbao, J. Effect of the Operating Conditions in the Transformation of DME to Olefins over a HZSM-5 Zeolite Catalyst. *Ind. Eng. Chem. Res.* **2016**, *55*, 6569–6578. [CrossRef]

40. Sierra, I.; Ereña, J.; Aguayo, A.T.; Arandes, J.M.; Olazar, M.; Bilbao, J. Co-Feeding Water to Attenuate Deactivation of the Catalyst Metallic Function (CuO–ZnO–Al_2O_3) by Coke in the Direct Synthesis of Dimethyl Ether. *Appl. Catal. B Environ.* **2011**, *106*, 167–173. [CrossRef]

41. Gayubo, A.G.; Aguayo, A.T.; Del Campo, A.E.S.; Tarrío, A.M.; Bilbao, J. Kinetic Modeling of Methanol Transformation into Olefins on a SAPO-34 Catalyst. *Ind. Eng. Chem. Res.* **2000**, *39*, 292–300. [CrossRef]

42. Cordero-Lanzac, T.; Aguayo, A.T.; Gayubo, A.G.; Bilbao, J. Consideration of the Activity Distribution Using the Population Balance Theory for Designing a Dual Fluidized Bed Reactor-Regenerator System. Application to the MTO Process. *Chem. Eng. J.* **2021**, *405*, 126448. [CrossRef]

43. Portillo, A.; Ateka, A.; Ereña, J.; Aguayo, A.T.; Bilbao, J. Conditions for the Joint Conversion of CO_2 and Syngas in the Direct Synthesis of Light Olefins Using In_2O_3–ZrO$_2$/SAPO-34 Catalyst. *Ind. Eng. Chem. Res.* **2021**, *2022*, 10365–10376. [CrossRef] [PubMed]

44. Ghasemi, M.; Mohammadi, M.; Sedighi, M. Sustainable Production of Light Olefins from Greenhouse Gas CO_2 over SAPO-34 Supported Modified Cerium Oxide. *Microporous Mesoporous Mater.* **2020**, *297*, 110029. [CrossRef]

45. Sánchez-Contador, M.; Ateka, A.; Aguayo, A.T.; Bilbao, J. Direct Synthesis of Dimethyl Ether from CO and CO_2 over a Core-Shell Structured CuO-ZnO-ZrO$_2$@SAPO-11 Catalyst. *Fuel Process. Technol.* **2018**, *179*, 258–268. [CrossRef]

46. Frei, M.S.; Capdevila-Cortada, M.; García-Muelas, R.; Mondelli, C.; López, N.; Stewart, J.A.; Ferré, D.C.; Pérez-Ramírez, J. Mechanism and Microkinetics of Methanol Synthesis via CO_2 Hydrogenation on Indium Oxide. *J. Catal.* **2018**, *361*, 313–321. [CrossRef]
47. Chen, T.Y.; Cao, C.; Chen, T.B.; Ding, X.; Huang, H.; Shen, L.; Cao, X.; Zhu, M.; Xu, J.; Gao, J.; et al. Unraveling Highly Tunable Selectivity in CO_2 Hydrogenation over Bimetallic In-Zr Oxide Catalysts. *ACS Catal.* **2019**, *9*, 8785–8797. [CrossRef]